RSC Advances

PAPER

View Article Online
View Journal | View Issue

Cite this: *RSC Adv.*, 2023, **13**, 22226

Influence of halogen elements in organic salts on n-type doping of CNT yarn for thermoelectric applications†

Aghnia Dinan Maulani Heriyanto, Yongyoon Cho,* Naofumi Okamoto, Ryo Abe, Manish Pandey, Hiroaki Benten and Masakazu Nakamura*

Received 5th June 2023
Accepted 5th July 2023

DOI: 10.1039/d3ra03755j

rsc.li/rsc-advances

Doping control of carbon nanotube (CNT) is crucial for thermoelectric (TE) application to maximize the power conversion efficiency. Despite the recent achievement of good air stability by organic salts for n-type carrier doping, their doping mechanism has not been systematically investigated so far. Here, we demonstrate doping of CNT yarn using ammonium salts with different halogen elements (tetrabutylammonium salts, TBAX where X = Cl, Br, or I) through the dipping technique. By changing the halogen element, we specifically investigated the halogen effect in the n-type doping process of CNT. The introduction of each material into the CNT yarn and its doping reaction were then studied by energy-dispersive X-ray spectroscopy and X-ray photoelectron spectroscopy. Halogen element was found to affect the excess amount of TBA^+ cation in the CNT yarn. The largest amount of excess TBA^+ is found in the TBAI-doped yarn, which stabilizes the most amount of negative charge in CNT, enhancing the TE performance and its stability over one month in air. This study discovers the importance of the halogen element in the doping process of CNT-based TE materials by organic salts, simultaneously offering an efficient and stable n-type doping strategy.

1 Introduction

Organic thermoelectric (TE) devices have been attracting research interest by directly converting waste heat to electricity, especially for flexible energy harvesting field.[1–8] Among the potentially suitable materials for thermoelectric generators, carbon nanotube (CNT)[9,10] has emerged due to its high electrical conductivity, mechanical robustness, flexibility, lightweight, and solution processing capability. The efficiency of TE materials is generally evaluated by the dimensionless figure of merit (ZT), which is defined as $ZT = \alpha^2\sigma T/\kappa$, where α, σ, T and κ are Seebeck coefficient, electrical conductivity, absolute temperature and thermal conductivity, respectively, and the factor $\alpha^2\sigma$ is frequently referred to as power factor (PF).[11] In general, high Seebeck coefficient, high electrical conductivity, and low thermal conductivity are prerequisites for high TE performance. Although CNT-based materials show relatively high σ values, they also show high κ values,[12–14] which is not beneficial for high TE performance. Therefore, it is necessary to reduce the thermal conductivity of CNTs by forming a composite, as has been done by several researchers.[15–17]

Another important method to enhance CNT's TE performance is optimizing carrier concentration by doping.[18,19] Generally, doping mechanisms can be categorized into two types – 'charge transfer' between host and dopant by adding neutral dopant molecules having sufficiently different electronegativity against CNT and 'charge stabilization' by adding permanent ions as a guest, which may be stabilized initially with volatile counter ions, resulting in the counter ionization of CNT to maintain electrical neutrality (Fig. 1).[20–25] For example, Ali *et al.*[20] and Myint *et al.*[21] reported a charge transfer method by adding 2,3,5,6-tetrafluoro-tetracyanoquinodimethane (F4TCNQ) into CNT and show good p-type TE performance due to the charge transfer from the CNT's valence band maximum (VBM) to the lower LUMO level of the dopant (Fig. 1(a1)). Compared to such p-type doping, n-type doping by the charge transfer method is generally challenging because it is difficult to obtain stable and strong electron donors.[26–28] On the other hand, the charge stabilization method using poly(diallyldimethylammonium chloride) (PDDA) was used for n-type doping by Jang *et al.* (Fig. 1(b2)).[25] Although various works have been done for n-type doping, performance of the n-type-doped CNTs still lag behind[22,29–33] because the unintentional p-type doping to semiconducting CNTs under ambient atmosphere tends to override the n-type doping[34,35] Therefore, finding an effective and stable n-type doping technique is necessary to obtain practical CNT-based TE devices.

Division of Materials Science, Nara Institute of Science and Technology, 8916-5 Takayamacho, Ikoma, Nara 630-0192, Japan. E-mail: yy.cho@ms.naist.jp; mnakamura@ms.naist.jp

† Electronic supplementary information (ESI) available. See DOI: https://doi.org/10.1039/d3ra03755j

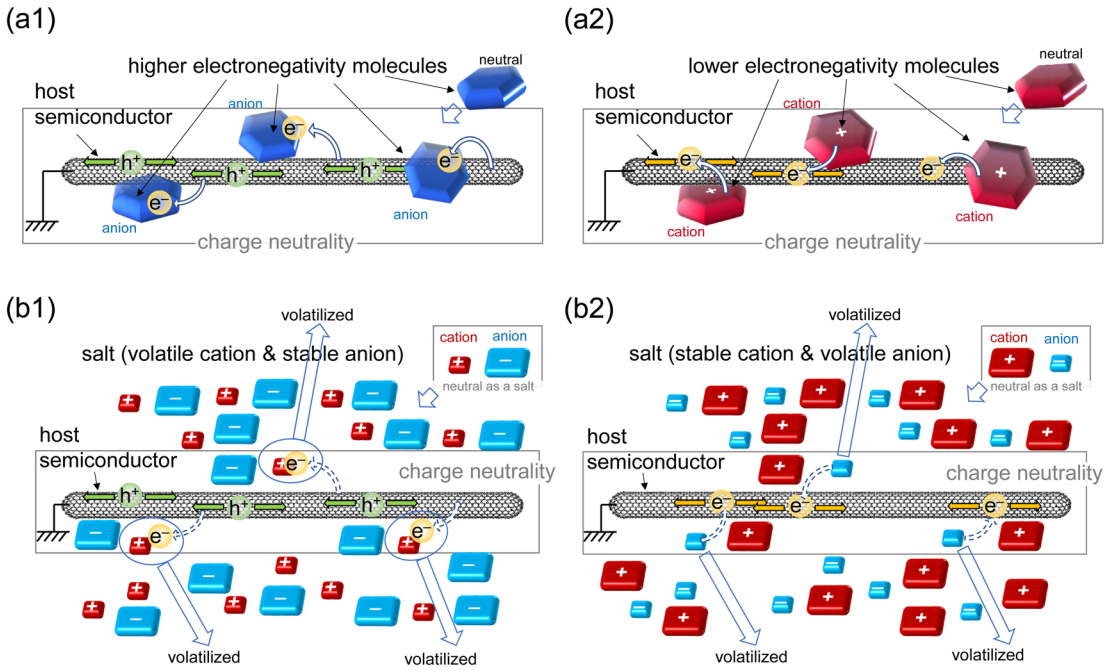

Fig. 1 Two types of popular chemical doping mechanisms: (a1 and a2) 'charge transfer' between host and dopant by adding neutral dopant molecules having sufficiently different electronegativity, and (b1 and b2) 'charge stabilization' by adding permanent ions, or unbalanced salt, as a guest resulting in the counter ionization of the conducting host to maintain charge neutrality. The charge transfer between the host and guest in the charge stabilization mechanism (b1 or b2) does not necessarily occur directly between them, (a1) and (b1) are for p-type doping and (a2) and (b2) for n-type doping.

Between two types of doping above, the charge stabilization has an advantage in terms of long-term stability of TE device which is because the large pool of anion–cation pairs, of which net charge is natural, can be a continuous source of doping reaction when the permanent charge due to the unbalanced anion or cation decreases with time. Some researchers employed the charge stabilization doping by organic salt such as tetra-butylammonium salt (TBABr)[23] and cetyltrimethylammonium bromide (CTABr)[36] and obtained good stability in n-type CNT without encapsulation. In Cheng's report,[36] they carried out two kinds of experiments, first used tetramethylammonium (TMA) salts with three halogen anions (Cl^-, Br^-, and I^-) and showed a significant effect on the TE performance in every sample. Second, they used three types of cations, TMABr, octyltrimethylammonium bromide (OTABr), and CTABr showed no distinct effect on the TE performance. However, how the halogen type influences on the TE performance has not been sufficiently investigated and the doping mechanism of the organic salt with halogen is still unclear. Additionally, their work did not address the problem of high thermal conductivity in CNTs.

Another missing viewpoint is that most doping works are carried out using CNT thin films,[23,37–40] possibly due to the easiness of fabrication. However, thick film-type samples are not facile to apply for wearable TE devices due to the lack of flexibility and difficulty in fabrication. An innovative pathway is a yarn-type sample of which the advantages are not only the flexibility,[41–43] but also the ability for a millimetre-order-thick flexible device which is easy to obtain large temperature difference even by natural air cooling, as demonstrated in previous studies.[11,15,20] CNT yarns also hold benefits in the complex device design in the integrated fabrics.[15,44] Therefore, it is worthwhile to develop a strategy to effectively optimize the thermoelectric properties of CNT yarns.

Based on the above background, we conducted a systematic study and solved the high thermal conductivity in CNT by composite form by adding organic salts composed of relatively large organic cations and various halogen anions. In this work, neat CNT yarns as starting samples were made without any binder polymers and the excess amount of surfactant, which is used to stabilize the CNT ink, was also removed from the yarn as possible as we can. As a result of the removal of electron withdrawing impurities in the CNT yarn and a help of the minimum amount of surfactant, it exhibited n-type thermoelectric properties. This is expected to simplify the doping behaviour in this work as simple as possible. Tetra-butylammonium salts (TBAX where X = Cl, Br, or I) were incorporated by dipping the CNT yarns into *N*,*N*-dimethylformamide (DMF) solution of TBAX. We then systematically investigated the change in the composition and thermoelectric properties of the CNT yarns by different halogen elements using X-ray photoelectron spectroscopy (XPS) and other techniques to understand the doping mechanism. Changing the halogen element has affected the amount of TBA^+ and X^- incorporated in the yarn. Hence, the optimal n-type CNT yarn was found in TBAI-doping with highest amount of excess TBA^+ which plays the most important role in n-type doping by the charge stabilization method (Fig. 1(b2)). TBAX was also found to decrease the thermal conductivity of CNT yarns. Thus,

TBAI-doped CNT yarn fabricated by the dipping method achieved a *ZT* value of 0.0034, which is around 3 times higher than that of pristine CNT yarn.

2 Experimental

2.1 Materials

The SWCNTs (e-DIPS, diameter 1.5 nm, purity of carbon >90%) were purchased from Meijo Nano Carbon. All the chemicals are used without further purification in the experiments. Tetrabutylammonium chloride, bromide, and iodide (TBACl, TBABr, and TBAI, respectively) were purchased from Tokyo Chemical Industry (TCI). *N*,*N*-dimethylformamide (DMF) was also purchased from TCI. Surfactant (Emulgen 350) and ionic liquid (IL) 1-butyl-3-methylimidazolium hexafluorophosphate (BMIM-PF6) were purchased from Kao Chemicals and Merck, respectively.

2.2 Methods

Three mg of the raw CNT material was primarily dispersed in IL with 4 wt% surfactant by an agate mortar for 1 hour to disentangle the CNT bundles. Then, the IL was extracted from the CNT dispersion by 3 times of centrifugation (3000 rpm for 1 minute). Next, the CNT was dispersed by ultrasonic application treatment (Branson) for 1 min. Then, the CNT dispersion was injected into a methanol coagulation bath to form gel-like yarn and left for 24 hours to remove excess surfactant. The gel-like yarn was subsequently pulled up slowly and dried in air at room temperature. After drying, the yarn was annealed at a temperature of 300 °C for 2 hours to further remove the surfactant and water.

The TBAX solutions (X = Cl, Br, or I) were fabricated by dissolving in DMF with 0.54 M concentration, stirring for 3 hours. Doping treatment was carried out by dipping a CNT yarn into TBAX solutions for 90 minutes under inert atmosphere. An experimental procedure for the doping process of CNT yarn with TBAX can be seen in Fig. S1(a).†

2.3 Characterization

The prepared CNT yarn (with diameter around 80 μm) was cut into 35 mm long and fixed to four electrode blocks on a sapphire substrate with silver paste (Fig. S1(b)†). The *I*–*V* characteristics to calculate electrical conductivity were measured with the four-probe method. Seebeck coefficient was measured using the voltage and temperature difference between the two voltage-measurement electrodes under application of temperature gradient in the lateral direction of Fig. S1(b).† Seebeck coefficients were measured at room temperature. The temperature difference between the two voltage-measurement electrodes was initially set at 0 K and varied in 0.5 K increments up to 2 K. The temperature difference was measured by two thermocouples bonded at the dummy electrodes near the voltage-measurement electrodes. The electromotive force was measured for 3 minutes at each temperature difference. The thermal diffusivity was measured with a scanning laser heating AC method (Laser PIT, Advance Riko). Thermal conductivity was measured by the DC heating cross-junction method which is a modified version of the DC heating T-type method.[45] In this method, a Pt heating/sensing wire and a single yarn are mounted in a cross geometry (Fig. S1(c)†). Since no electrical current is applied to the CNT yarn, the influences of the contact resistance and instability of the sample resistance are ignored.

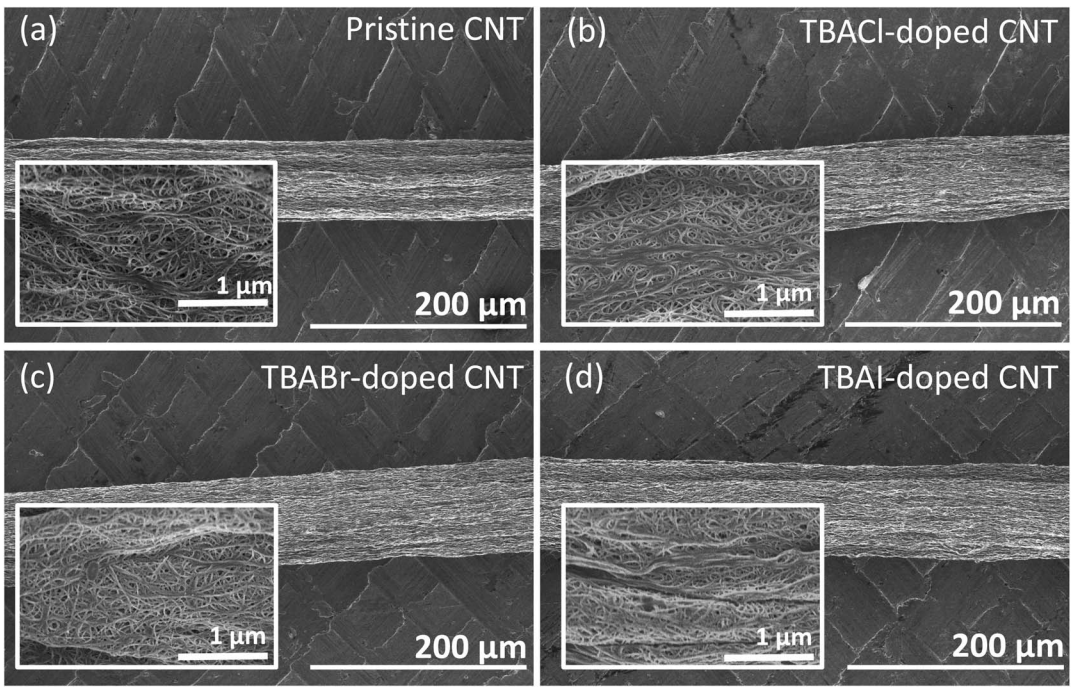

Fig. 2 SEM images of (a) pristine, (b) TBACl-, (c) TBABr-, and (d) TBAI-doped CNT yarns. Inset is a magnified image of each yarn.

Raman spectroscopy, X-ray photoelectron spectroscopy (XPS), scanning electron microscopy (SEM), and Energy Dispersive X-ray Spectroscopy (EDX) were measured using NRS-4100-30 (JASCO), PHI 5000 VersaProbeII (ULVAC-PHI), and SU9000 (Hitachi), respectively.

3 Results and discussion

Detailed information regarding the materials, experimental methods, and structural determination are explained in the ESI.† A dipping method, which has been already proven by other researchers,[46,47] was used for the doping step. No morphological difference before and after the doping was found in the scanning electron microscopy (SEM) images shown in Fig. 2(a)–(d), indicating that the doping agents used in this work do not deform the CNT yarn. In high-magnification images (insets in Fig. 2(a)–(d)), the CNT bundle networks were clearly seen on all of the yarns, indicating that the salts were not crystalized on the yarn surface but infiltrated into the yarn and/or adsorbed on the bundle surface as very thin films. To confirm the incorporation of the dopant in the yarn, energy dispersive X-ray spectroscopy (EDX) analysis was performed, of which results are shown in Fig. S2.† The results indicated that a sufficient amount of TBAX had been incorporated into the yarn by the simple dipping method.

To evaluate the doping effect of TBAX, α and σ are analysed for the TBAX-doped CNT yarns using a four-probe method.[48] Before the comparison of halogen elements, we measured the Seebeck coefficient of a pristine yarn under air and vacuum conditions, both of which exhibited negative values (Fig. S3†). The negative value of Seebeck coefficient for pristine CNT could be also from the effect of the surfactant used in the yarn fabrication, Emulgen, as we previously reported.[11] Although the measured values are not so different, the Seebeck coefficients shown in this work were measured under a vacuum to exclude the environmental effect due to the variation in the environmental humidity.[31,49] Thermoelectric characteristics of the TBAX-doped CNT yarns are presented in Fig. 3(a)–(c). All of the dopant seems to increase the free electron concentration in the CNT yarn resulting in the increase of electrical conductivity from that of the pristine one. TBAI-doped CNT yarn showed the highest electrical conductivity (1160 S cm^{-1}) among them. Although the carrier concentration seemed to be increased in the doped samples, the Seebeck coefficients remained almost constant. Generally, increase of carrier concentration of a semiconductor would affect its Seebeck coefficient, as it is commonly known that the Seebeck coefficient decreases with exponential increase in carrier density.[50] However, such a trend was not found in this experiment where Seebeck coefficient of doped CNTs did not decrease from that of the pristine one (Fig. 3(b)), implying that the carrier concentration is varied within the range where Seebeck coefficient exhibits its broad peak value.[51] The maximum PF of 351 μW mK^{-2} was obtained in the TBAI-doped CNT yarn (Fig. 3(c)).

We further evaluated the thermal transport properties along the longitudinal direction of the yarn. Fig. 3(d) shows the result of the κ measurement. The incorporation of TBAX to the CNT

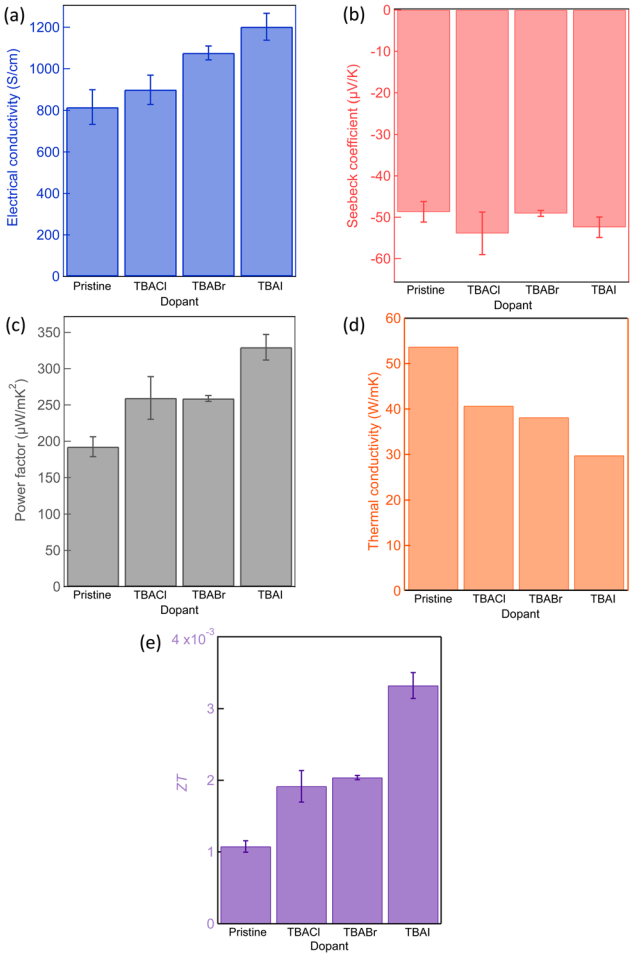

Fig. 3 Thermoelectric properties of pristine and doped CNT yarns: (a) electrical conductivity, (b) Seebeck coefficient, (c) power factor, (d) thermal conductivity, and (e) *ZT*. The error bar indicates the standard deviation of the measured values for three samples.

generally reduced κ. The κ value of TBAI-doped CNT is 1.8 times less (29.7 W mK^{-1}) than that of the pristine one. The possible origin of the κ decrease is that the TBAX molecules are positioned at the CNT-bundle/CNT-bundle junctions blocking the heat transport and/or at the CNT surface, disturbing the intra-CNT phonon transport.[52] The disturbance of phonon propagation was also supported by lowered thermal diffusivity than that of the pristine CNT sample (Fig. S4†), On the basis of measured κ, we calculated *ZT* values (Fig. 3(e)), exhibiting 3-fold improvement (0.0033) than that of the pristine CNT (0.0011). Consequently, we found that the combinational effect in σ and κ has enhanced the *ZT* value of the CNT yarns by selecting the appropriate organic salts.

To investigate the carrier doping mechanism by structural and compositional analyses, we first measured Raman spectra to examine the defects in CNT and the interaction between CNT and TBAX. In Fig. S5(a),† there is no differences in the G+ band peak position (1590 cm^{-1}) among all the yarns, indicating no formation of strong charge–transfer complex or lattice distortion. To evaluate the change of defect, we also calculated the

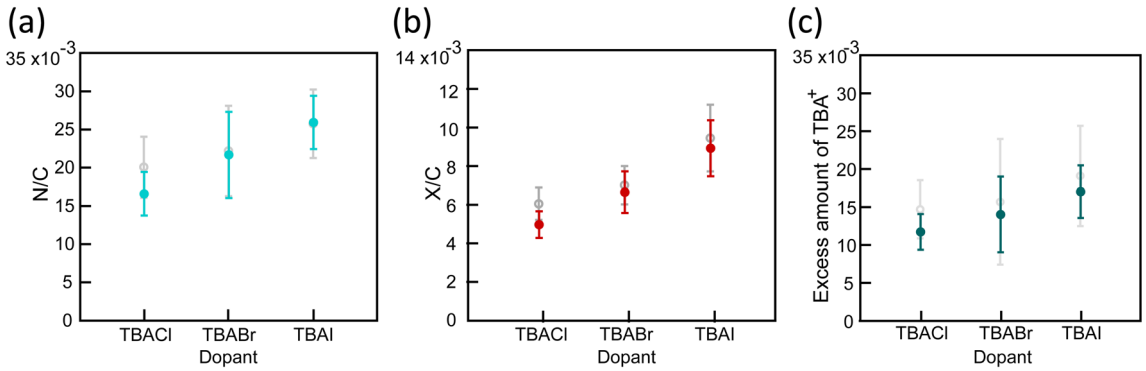

Fig. 4 Results of XPS analyses for TBAX-doped CNT yarns: (a) N *vs.* C atomic ratio, (b) halogen *vs.* C atomic ratio, and (c) excess TBA^+ calculated by (a and b). Two sets of data indicated with color and gray are calculated using two different definitions of sensitivity factors: (color) assuming that the dopant molecules exist only on the yarn surfaces and (gray) assuming a uniform distribution in thickness. The error bar indicates the standard deviation of the measured values for ten positions for each sample.

intensity ratio of the D (1340 cm^{-1}) and 2D (2690 cm^{-1}) bands against the G+ band as shown in Fig. S5(b) and (c).† The D/G+ ratios (often its inverse is known as the G/D ratio and hysterically used in nanocarbon community) of the doped CNT yarns have almost the same values compared with that of the pristine CNT yarn. 2D/G+ ratio also shows no difference. Therefore, we concluded that the increase in defect is not the origin of the variation of electrical or thermal conductivities by the TBAX doping.

X-ray photoelectron spectra (XPS) were measured to evaluate the chemical composition of the doped CNT yarns. By assessing the amount of TBA^+ cation and halogen anion in each sample, it is expected to determine the doping reaction and difference caused by the halogen element. N/C atomic ratio, which is directly indicative for TBA^+, was compared in Fig. 4(a). The atomic ratio is calculated from the intensities of N1s and C1s peaks using two types of the sensitivity factors of the XPS instrument. The estimated amount of nitrogen in each sample shows that TBAI-doped CNT has the largest quantity of TBA^+ than the others. This is further supported by the amount of excess sp^3 component than the pristine CNT yarn, which can be also attributed to the TBA^+ quantity. We separated the C1s peak into sp^3, sp^2, C–O, and π–π* shake-up peaks (Fig. S6(a)†). The sp^3 component is regarded as a combination of defects in CNT, small amount of residual surfactant, and carbons in TBA^+. Since the defect density in CNT is unchanged judging from the Raman results, we can estimate the amount of TBA^+ by:

$$\text{Amount of } TBA^+ = \frac{sp^3(\text{doped}) - \frac{sp^2(\text{doped}) + \pi - \pi^*(\text{doped})}{sp^2(\text{pristine}) + \pi - \pi^*(\text{pristine})} sp^3(\text{pristine})}{16} \quad (1)$$

From eqn (1), we estimated the amount of TBA^+ from the percent composition in Fig. S5a.† The result was consistent with the amount of nitrogen atoms, supporting that TBA^+ was largely incorporated when TBAI was used (Fig. S6a†). Fig. 4(a) and (b) clearly indicate that the N/C values are higher than the X/C values. X/C can be regarded as an adsorbed halogen atom on the CNT, whereas N/C is the total amount of TBA molecules. The difference in the amount implies that TBA^+ cations are more incorporated to CNT yarn than halogen anions. The excess amount of TBA^+ in CNT yarn was then calculated by subtracting X/C from N/C showing the result in the order of Cl < Br < I (Fig. 4(c)). The excess amount of TBA^+ was also plotted against the increase of σ in Fig. 5(a). This result implies that the increase of σ is roughly proportional to the excess amount of TBA^+ with a threshold value. This is consistent with the typical n-type doping effect by the charge stabilization method (Fig. 1(b2)) where excess cation stabilizes the negative charge carriers in CNT. The existence of the threshold is still an open question. It may be due to the electron traps that kills doped electrons or removal of already existing n-type dopants, such as Emulgen.

On the basis of the experimental results and discussion above, we can suggest the doping mechanism as:

$$aCNT + bTBA^+X^- \rightleftharpoons (a-c)CNT + (b-c)TBA^+X^- + cCNT^- + cTBA^+ + c1/2X_2 \quad (2)$$

When the TBAX molecule is dissolved in the solution, some proportion of TBAX would be adsorbed onto CNTs. Some TBA^+ from TBAX can stabilize the negative charge in CNT, and X^- could be dissociated and converted into X_2 after donating an electron to CNT. Detail of the electron transfer from halogen to CNT, whether it occurs directly or indirectly, has not been clarified yet. From eqn (2), the generated neutral halogen molecules should be expelled from the system during the dipping process. Some of the halogen molecules, for example Cl_2, may possibly evaporate from the dopant solution but the emission of halogen gas during the doping had not been

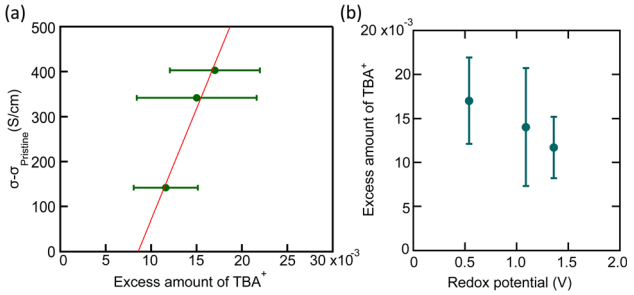

Fig. 5 (a) Relation between increase of electrical conductivity $\Delta\sigma$ (σ – σ pristine) and excess amount of TBA^+. (b) Relation between excess amount of TBA^+ and redox potential of halogens. Here, the average value by the two definitions of sensitivity factors in Fig. 4 is used for the excess amount of TBA^+.

Table 1 The redox potential of halogen[54]

Halogen element	Redox potential
$Cl_2 + 2e^- \rightleftharpoons 2Cl^-$	+ 1.36 V
$Br_2 + 2e^- \rightleftharpoons 2Br^-$	+ 1.09 V
$I_2 + 2e^- \rightleftharpoons 2I^-$	+ 0.54 V

detected by mass spectrometry (Fig. S7(a) and (b)†). This could be due to the small amount of generated halogen, which is lower than the detection limit of the instrument. Considering the doping process and the sensitivity of the mass spectrometer, the amount of solvent vapor is much more than generated halogens distributing ionization and detection of halogens (see detailed calculations in ESI†). This would be the origin of many peaks in Fig. S7,† which can be assigned mostly to the DMF mother and daughter ions instead of halogen. Moreover, other calculations of halogen generation based on charge carrier concentration and XPS result also indicate a comparatively small halogen amount generated (also in ESI†). Therefore, we speculate that the suggested reaction in eqn (2) can occur with a loss of the small amount of neutral halogen, corresponding to the excess amount of TBA^+. These results are also consistent with a previous report on n-type doping by the ionic liquid where the excess cation incorporated in the CNT solids stabilizes the negative charges in CNT. By this work, it has become more evident that the excess cation by losing counter anions caused the n-type doping effect to CNTs.[48,53]

Among the TBAXs tested in this work, TBAI produced the largest amount of excess TBA^+. This can be explained by the difference in the redox potential of the three halogen elements (Table 1). Iodine, having the lowest redox potential, prefers to be natural state than ionized state. Therefore, the eqn (2) should be more biased to the right-hand side in equilibrium. This suggests that TBAI is the strongest reducing agent during the doping process and will donate the most electrons to CNTs, become unstable in the adsorbed salt, and diffuse into the solution. Therefore, the amount of excess TBA^+ increases as the redox potential decreases, as shown in Fig. 5(b).

Another possible doping mechanism is the generation of polyhalide anions. However, it's contrary with XPS results of halide regions in TBAX-doped CNT yarn where only one component was observed for each halogen element (Fig. S9†). The XPS spectra of the I3d region exhibit clear doublet with peaks registered close to 618.5 and 630.1 eV corresponding to the $I3d_{5/2}$ and $I3d_{3/2}$ states, respectively.[55,56] The XPS spectra of Br3d and Cl2p also only showing the main peaks (67.52 eV, 68.553 eV) and (197.37 eV, 198.85 eV), respectively. These results suggest that polyhalide anions are not generated during the doping process.

Time-dependent changes of α, σ and PF were analysed to evaluate the stability of TBAX-doped CNT yarns under ambient conditions without any encapsulation treatment (Fig. 6(a)–(c)). Even after 864 hours (36 days), α and σ values of a TBAI-doped CNT yarn showed almost the same values resulting in the unchanged PF. As for TBABr- and TBACl-doped yarns, α and σ decreased by around 25% and 40%, respectively. These changes could be attributed to the adsorption amount of the doping agent, which can have a passivation effect against air. It could also be related to the material stability itself judging from the melting points of TBAX, which are in the order of TBACl < TBABr < TBAI.[57]

Furthermore, judging from the increase in Seebeck coefficient up to the initial 200 hours (Fig. 6(a)), it is highly probable that the large pool of salt was slowly developing a doping

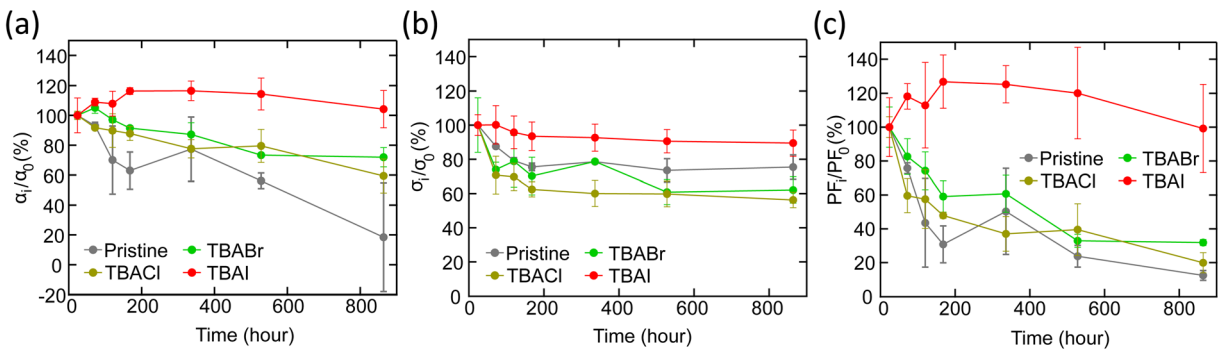

Fig. 6 Stability test of the TBAX-doped CNT yarns for 36 days in air: (a) Seebeck coefficient, (b) electrical conductivity, and (c) power factor. The error bar indicates the standard deviation of the results from three samples.

reaction and replenishing electrons in CNTs during the storage in the atmosphere. Thus, TBAI has achieved the highest stability in CNT compared to TBABr or TBACl. Consequently, the iodide compound was found to be the best material among halogen elements for n-type doping of CNT with the highest TE performance and stability.

4 Conclusions

A systematic study on the n-type doping of CNT yarn with TBAX which contains relatively large organic cation and various halogen anions was carried out. It was demonstrated that the TBAX effectively increased the electrical conductivity and decreased thermal conductivity of CNT yarns. Iodine was found to exhibit the best performance and stability among three halogen anions tested in this work. As a result, approximately three times higher *ZT* was obtained by the TBAI treatment compared to that of the pristine CNT yarn. Our study has also shed light on the doping mechanism of TBAX, which is influenced by the redox potential of halogen element. A lower redox potential led to a larger amount of excess TBA^+ that stabilizes the negative charges, that is, free electrons, in the CNT. This work suggests that the charge stabilization method using large organic cation and iodine would be a promising strategy for efficient and stable n-type doping of CNTs.

Author contributions

A. D. M. H. prepared the manuscript, analyzed the XPS and Raman data. Y. C. carried out and analyzed the gas-phase mass spectrometry, N. O. synthesized and characterized the pristine CNT yarns. A. D. M. H. and R. A. conducted the measurement of thermoelectric parameters. M. P. and H. B. contributed to the data analyses and interpretation, Y. C. and M. N. supervised the project. All authors have contributed to the final version of the manuscript.

Conflicts of interest

There are no conflicts to declare.

Acknowledgements

This work was supported by JST CREST Grant Number JPMJCR18I3, Japan and Hirose Foundation, Japan. A. D. M. H. thanks Nikita Kumari for her insight in this manuscript.

References

1 Y. Xue, C. Gao, L. Liang, X. Wang and G. Chen, *J. Mater. Chem. A*, 2018, **6**, 22381–22390.
2 C. Li, F. Jiang, C. Liu, W. Wang, X. Li, T. Wang and J. Xu, *Chem. Eng. J.*, 2017, **320**, 201–210.
3 X.-L. Shi, J. Zou and Z.-G. Chen, *Chem. Rev.*, 2020, **120**, 7399–7515.
4 I. Petsagkourakis, K. Tybrandt, X. Crispin, I. Ohkubo, N. Satoh and T. Mori, *Sci. Technol. Adv. Mater.*, 2018, **19**, 836–862.
5 Y. Du, J. Xu, B. Paul and P. Eklund, *Appl. Mater. Today*, 2018, **12**, 366–388.
6 R. Tian, C. Wan, N. Hayashi, T. Aoai and K. Koumoto, *MRS Bull.*, 2018, **43**, 193–198.
7 N. Nandihalli, C. J. Liu and T. Mori, *Nano Energy*, 2020, **78**, 105186.
8 G. Prunet, F. Pawula, G. Fleury, E. Cloutet, A. J. Robinson, G. Hadziioannou and A. Pakdel, *Mater. Today Phys.*, 2021, **18**, 100402.
9 G. Lota, K. Fic and E. Frackowiak, *Energy Environ. Sci.*, 2011, **4**, 1592–1605.
10 J. Chen, J. Z. Wang, A. I. Minett, Y. Liu, C. Lynam, H. Liu and G. G. Wallace, *Energy Environ. Sci.*, 2009, **2**, 393–396.
11 Y. Cho, N. Okamoto, S. Yamamoto, S. Obokata, K. Nishioka, H. Benten and M. Nakamura, *ACS Appl. Energy Mater.*, 2022, **5**, 3698–3705.
12 M. Pandey, R. Abe, N. Okamoto, Y. Sekimoto, K. Nishioka, Y. Okajima and M. Nakamura, *Appl. Phys. Express*, 2020, **13**, 1–5.
13 S. Yamaguchi, I. Tsunekawa, N. Komatsu, W. Gao, T. Shiga, T. Kodama, J. Kono and J. Shiomi, *Appl. Phys. Lett.*, 2019, **115**, 223104.
14 B. Kumanek and D. Janas, *J. Mater. Sci.*, 2019, **54**, 7397–7427.
15 M. Ito, N. Okamoto, R. Abe, H. Kojima, R. Matsubara, I. Yamashita and M. Nakamura, *Appl. Phys. Express*, 2014, **7**, 1–4.
16 C. Yu, Y. S. Kim, D. Kim and J. C. Grunlan, *Nano Lett.*, 2008, **8**, 4428–4432.
17 C. K. Mai, B. Russ, S. L. Fronk, N. Hu, M. B. Chan-Park, J. J. Urban, R. A. Segalman, M. L. Chabinyc and G. C. Bazan, *Energy Environ. Sci.*, 2015, **8**, 2341–2346.
18 L. Tzounis, M. Liebscher, R. Fuge, A. Leonhardt and V. Mechtcherine, *Energy Build.*, 2019, **191**, 151–163.
19 T. Zuo, J. Li, Z. Gao, Y. Wu, L. Zhang, B. Da, X. Zhao and L. Xiao, *Mater. Today Commun.*, 2020, **23**, 100907.
20 M. K. Ali, N. Okamoto, R. Abe, M. Pandey, A. A. Moneim and M. Nakamura, *Synth. Met.*, 2021, **280**, 116874.
21 M. T. Z. Myint, T. Nishikawa, H. Inoue, K. Omoto, A. K. K. Kyaw and Y. Hayashi, *Org. Electron.*, 2021, **90**, 106056.
22 Y. Nonoguchi, M. Nakano, T. Murayama, H. Hagino, S. Hama, K. Miyazaki, R. Matsubara, M. Nakamura and T. Kawai, *Adv. Funct. Mater.*, 2016, **26**, 3021–3028.
23 R. Chen, J. Tang, Y. Yan and Z. Liang, *Adv. Mater. Technol.*, 2020, **5**, 1–7.
24 M. Nakano, T. Nakashima, T. Kawai and Y. Nonoguchi, *Small*, 2017, **13**(29), 1700804.
25 W. Jang, H. A. Cho, K. Choi and Y. T. Park, *Micromachines*, 2018, **9**(12), 628.
26 Y. Zhang, B. De Boer and P. W. M. Blom, *Phys. Rev. B: Condens. Matter Mater. Phys.*, 2010, **81**, 1–5.
27 C. K. Chan, W. Zhao, S. Barlow, S. Marder and A. Kahn, *Org. Electron.*, 2008, **9**, 575–581.
28 W. Walukiewicz, *Phys. B*, 2001, **303**, 123–134.

29 G. Zuo, Z. Li, E. Wang and M. Kemerink, *Adv. Electron. Mater.*, 2018, **4**, 1–6.
30 K. Bradley, S. H. Jhi, P. G. Collins, J. Hone, M. L. Cohen, S. G. Louie and A. Zettl, *Phys. Rev. Lett.*, 2000, **85**, 4361–4364.
31 A. Zettl, *Science*, 2000, **287**, 1801–1804.
32 C. K. Mytafides, L. Tzounis, G. Karalis, P. Formanek and A. S. Paipetis, *ACS Appl. Mater. Interfaces*, 2021, **13**, 11151–11165.
33 M. Yarali, J. Hao, M. Khodadadi, H. Brahmi, S. Chen, V. G. Hadjiev, Y. J. Jung and A. Mavrokefalos, *RSC Adv.*, 2017, **7**, 14078–14087.
34 J. Zhang, K. Tse, M. Wong, Y. Zhang and J. Zhu, *Front. Phys.*, 2016, **11**(6), 117405.
35 K. Walzer, B. Männig, M. Pfeiffer and K. Leo, *Chem. Rev.*, 2007, **107**, 1233–1271.
36 X. Cheng, X. Wang and G. Chen, *J. Mater. Chem. A*, 2018, **6**, 19030–19037.
37 B. Kumanek, G. Stando, P. Stando, K. Matuszek, K. Z. Milowska, M. Krzywiecki, M. Gryglas-Borysiewicz, Z. Ogorzałek, M. C. Payne, D. MacFarlane and D. Janas, *Sci. Rep.*, 2021, **11**, 8649.
38 S. Hata, T. Mihara, M. Shiraishi, Y. Yamaguchi, Y. Du, Y. Shiraishi and N. Toshima, *Jpn. J. Appl. Phys.*, 2020, **59**, SDDD05.
39 L. Wang, Q. Yao, H. Bi, F. Huang, Q. Wang and L. Chen, *J. Mater. Chem. A*, 2015, **3**, 7086–7092.
40 F. Erden, H. Li, X. Wang, F. K. Wang and C. He, *Phys. Chem. Chem. Phys.*, 2018, **20**, 9411–9418.
41 J. Lee, D. M. Lee, Y. K. Kim, H. S. Jeong and S. M. Kim, *Small*, 2017, **13**, 1–8.
42 N. Behabtu, C. C. Young, D. E. Tsentalovich, O. Kleinerman, X. Wang, A. W. K. Ma, E. A. Bengio, R. F. Ter Waarbeek, J. J. De Jong, R. E. Hoogerwerf, S. B. Fairchild, J. B. Ferguson, B. Maruyama, J. Kono, Y. Talmon, Y. Cohen, M. J. Otto and M. Pasquali, *Science*, 2013, **339**, 182–186.
43 D. E. Tsentalovich, R. J. Headrick, F. Mirri, J. Hao, N. Behabtu, C. C. Young and M. Pasquali, *ACS Appl. Mater. Interfaces*, 2017, **9**, 36189–36198.
44 K. T. Park, T. Lee, Y. Ko, Y. S. Cho, C. R. Park and H. Kim, *ACS Appl. Mater. Interfaces*, 2021, **13**, 6257–6264.
45 R. Abe, Y. Sekimoto, S. Saini, K. Miyazaki, Q. Li, D. Li, K. Takahashi, T. Yagi and M. Nakamura, *J. Therm. Sci.*, 2022, **31**, 1037–1051.
46 E. Y. Jang, T. J. Kang, H. W. Im, D. W. Kim and Y. H. Kim, *Small*, 2008, **4**, 2255–2261.
47 C. Deetuam, D. Weise, C. Samthong, P. Praserthdam, R. R. Baumann and A. Somwangthanaroj, *J. Appl. Polym. Sci.*, 2015, **132**, 1–9.
48 M. Ito, T. Koizumi, H. Kojima, T. Saito and M. Nakamura, *J. Mater. Chem. A*, 2017, **5**, 12068–12072.
49 M. B. Jakubinek, M. A. White, G. Li, C. Jayasinghe, W. Cho, M. J. Schulz and V. Shanov, *Carbon*, 2010, **48**, 3947–3952.
50 H. J. Goldsmid, Thermoelectric Properties of Metals and Semiconductors, in *Introduction to Thermoelectricity*, Springer, Berlin, Heidelberg, 2016.
51 K. Yanagi, S. Kanda, Y. Oshima, Y. Kitamura, H. Kawai, T. Yamamoto, T. Takenobu, Y. Nakai and Y. Maniwa, *Nano Lett.*, 2014, **14**, 6437–6442.
52 A. D. Avery, B. H. Zhou, J. Lee, E. Lee, E. M. Miller, R. Ihly, D. Wesenberg, K. S. Mistry, S. L. Guillot, B. L. Zink, Y. Kim, J. L. Blackburn and A. J. Ferguson, *Nat. Energy*, 2016, **1**(4), 16033.
53 J. Jung, E. Hyun Suh, Y. Jeong, D. J. Yun, S. Chan Park, J. Gyu Oh and J. Jang, *Chem. Eng. J.*, 2022, **438**, 135526.
54 F. Gossenberger, T. Roman and A. Groß, *Electrochim. Acta*, 2016, **216**, 152–159.
55 G. Kalita, K. Wakita, M. Takahashi and M. Umeno, *J. Mater. Chem.*, 2011, **21**, 15209–15213.
56 Q. Han, C. Hu, F. Zhao, Z. Zhang, N. Chen and L. Qu, *J. Mater. Chem. A*, 2015, **3**, 4612–4619.
57 TCI Co catalogue, **https://www.tcichemicals.com/assets/brochure-pdfs/Brochure_Q6003_E.pdf**, accessed 10 May 2023.